Photochemistry

Deutsche Ausgabe: DOI: 10.1002/ange.201504518
Internationale Ausgabe: DOI: 10.1002/anie.201504518

White-Light Emission from an Integrated Upconversion Nanostructure: Toward Multicolor Displays Modulated by Laser Power

*Cheng Zhang, Liang Yang, Jun Zhao, Bianhua Liu, Ming-Yong Han, and Zhongping Zhang**

Abstract: *The white backlight in displays is generated by optimizing the proportions of individual emitters with different wavelengths by variations in materials composition, phase, and structure. Color pixels usually result from the separation of white light or the excitation with multiwavelength or multipulse sources. However, it is a challenge to develop a material that comprises a single structure and emits over the full visible spectrum, but where the emission wavelengths can be controlled by a simple excitation source. Herein, we report an upconversion nanostructure that incorporates several lanthanide ions in the same core@shell@shell structure. The combination of multiple narrow spectral bands results in the emission of white light. The emission colors can be tuned by changing the excitation power density, which manipulates the photon transfer pathways. Applications such as flat-panel displays and imaging have been demonstrated.*

The separation of white light into its components has been widely adopted in modern displays to obtain pure red-green-blue (RGB) colors for pixels.[1] The white backlight usually originates from a mixture of RGB materials in a strict proportion; these materials may be organic dyes,[2] quantum dots,[3] or upconversion nanocrystals.[4] To produce white light, mixed dyes are simultaneously excited by a source with a wide range of frequencies, while mixed quantum dots are simultaneously excited by a single-wavelength source because of their wide and narrow spectral bandwidths, respectively, and their different optimal excitation conditions. However, when these mixed emitters are present in one system, problems can be encountered with phase separation and energy transfer, which often lead to inconsistent color brightness and short lifespan. Herein, we report an integrated upconversion nanostructure that can emit RGB colors that cover the full visible range and can be combined to produce white light. This alternative strategy can be applied to display technology through controlling the output of the emission colors by using a simple excitation source instead of color separation.

The emission colors of materials intrinsically depend on their energy band levels, and the structure-based luminescence shows a characteristic spectrum for each material. Research has already been devoted to making materials with fixed structures emit different colors by electric bias or multiple-pulse excitations.[5] Currently, the most popular method is the individual synthesis of RGB-emitting materials with varying compositions, phases, and sizes. For example, the sequential emission colors of quantum dots from blue to red requires extremely strict size control over a very narrow range of 2–6 nm.[6] In order to obtain a single white-light-emitting material, the different RGB emitters should be incorporated into a consistent crystalline structure; however the overlapping of energy bands and the interference of photon transitions must be avoided for the independent emissions from each chromophore. In particular, a white-light-emitting material also needs balanced emission intensities for RGB light. To meet these requirements, ion-based emission centers may be preferred because the doping of multiple ions can be controlled in a feasible manner.[7]

With their many ladderlike 4f energy configurations, lanthanide ions can emit various colors that span the whole visible range.[4,8] Besides their narrow emission bands that result in pure colors, a remarkable advantage is that the luminescence of different lanthanide ions may be excited at the same near-infrared wavelength through multiphoton processes. Upon co-doping lanthanide ions into a single crystalline structure, the cross-relaxation and quenching of photon transitions generally limits the independent emissions and spectral intensities of these ions.[7a] In the present work, an integrated full-spectral upconversion nanostructure was prepared by optimizing the pathways of photon transitions from a set of selected lanthanide ions. The RGB emitters exhibited different spectral sensitivities to the excitation laser power density and thus allowed the modulation of a wide range of emission colors. The bright upconverted white light and the tunable emission color will be important in display technology and imaging.

Our designed $NaGdF_4$:Yb/Tm/Er@$NaGdF_4$:Eu@$NaYF_4$ nanostructure accommodates six kinds of lanthanide ions to obtain white light by upconversion (Figure 1a). Hexagonal-phase $NaGdF_4$ was chosen as the host for lanthanide ions because of its high upconversion efficiency.[8b] Yb^{3+} ions were chosen as sensitizers to absorb the near-infrared laser light, and Tm^{3+} and Er^{3+} were chosen as the origins of blue and green emissions, respectively. The Tm^{3+} and Er^{3+} ions were

[*] C. Zhang, L. Yang, J. Zhao, B. Liu, Dr. M. Han, Prof. Z. Zhang
Institute of Intelligent Machines
Chinese Academy of Sciences
Hefei, Anhui 230031 (China)
E-mail: zpzhang@iim.ac.cn
C. Zhang, L. Yang, Prof. Z. Zhang
Department of Chemistry
University of Science and Technology of China
Hefei, Anhui 230026 (China)
Dr. M. Han
Institute of Materials Research and Engineering, A*STAR
3 Research Link, Singapore 117602 (Singapore)
Prof. Z. Zhang
State Key Laboratory of Transducer Technology
Chinese Academy of Sciences, Hefei, Anhui 230031 (China)

Supporting information for this article is available on the WWW under http://dx.doi.org/10.1002/anie.201504518.

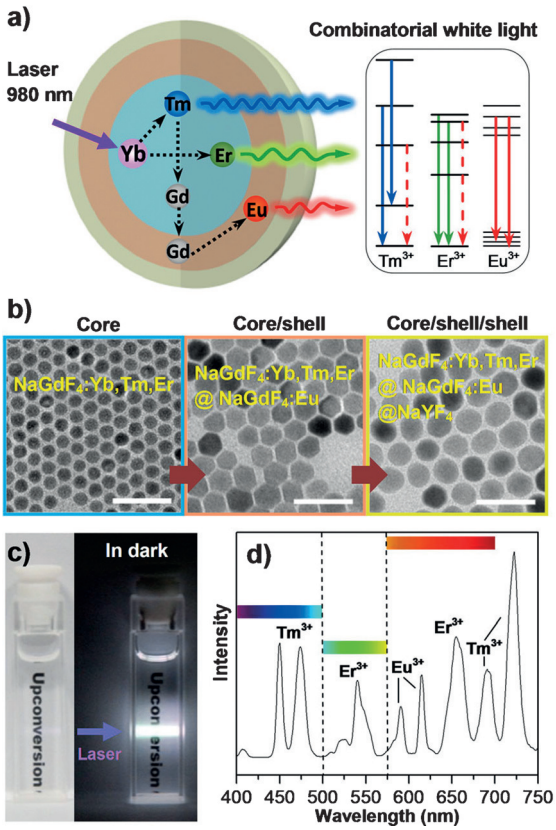

Figure 1. a) White-light-emitting nanostructure and simplified energy level diagram of blue, green, and red emissions. b) Typical growth process shown by transmission electron microscopy (TEM) images. c) Luminescence of nanocrystals in cyclohexane (1 mg mL^{-1}). Left: Photograph taken in daylight shows the transparency of the solution. Right: Under excitation with a 980 nm laser with a power density of 15 W cm^{-2}, the solution emits bright white light in the dark. d) Upconversion spectrum.

co-doped into $NaGdF_4$ core, and the Eu^{3+} ions, which are the origin of the red emission, were incorporated into the middle ($NaGdF_4$) shell. The outermost ($NaYF_4$) shell was necessary for minimizing the surface quenching and thus improving the emission intensities.[9] As shown by the TEM images in Figure 1 b, the $NaGdF_4$:Yb/Tm/Er cores with a size of around 11 nm were highly spherical and dispersive. After the $NaGdF_4$:Eu shells were coated onto the $NaGdF_4$:Yb/Tm/Er cores, the particle shapes became hexagonal with a size of 19 nm, thus suggesting the crystalline growth of $NaGdF_4$:Eu. Finally, the 2 nm $NaYF_4$ layer was further grown to form the outermost shell, and the resulting product comprised spherical nanocrystals approximately 23 nm in diameter. The detailed structural characterization is shown in Figures S1 and S2 in the Supporting Information.

The nanocrystals emit very bright white light under excitation by a 980 nm laser with a power density of 15 W cm^{-2} (Figure 1 c). The white light results from the combination of multiple narrow emission processes spanning the whole visible range from 400–750 nm (Figure 1 d). The main emissions from the $NaGdF_4$:Yb/Tm/Er core are in the blue (450 nm, 475 nm) and green (540 nm) regions, and arise from the $^1D_2 \rightarrow {}^3F_4$ and $^1G_4 \rightarrow {}^3H_6$ transitions of Tm^{3+} and the $^4S_{3/2} \rightarrow {}^4I_{15/2}$ transition of Er^{3+}, respectively. The Eu^{3+} ions in the $NaGdF_4$:Eu shell contribute their typical red emission at 590 nm ($^5D_0 \rightarrow {}^7F_1$) and 614 nm ($^5D_0 \rightarrow {}^7F_2$). Coating of the $NaGdF_4$:Eu shell with $NaYF_4$ also enhances the blue and green emission intensity by around 20 times and enhances the combined RGB emission by around 2.5 times (Figure S3).

The white-light emission should arise from the optimization of RGB emission at the ideal doping concentrations. Although Tm^{3+} and Er^{3+} ions in the core emit blue and green light, respectively, the blue emission is in fact quenched by high concentrations of Er^{3+}, and thus only green emission is observed[10–11] because the excitation energy in the $^3H_4$ level of the Tm^{3+} ion may transfer to the $^4I_{9/2}$ level of the Er^{3+} ion (Figure S4). In contrast, only blue emission is observed at a low Er^{3+} concentration. Here, an ideal proportion of 0.5 mol% Tm^{3+} to 0.05 mol% Er^{3+} was established to ensure the optimal intensities of the blue and green components in white light (Figure S5).

Tm^{3+} and Er^{3+} ions can also emit in the red region (Figure 1 a), but these signals are too weak to produce white light together with their blue and green emissions (Figure S6). Eu^{3+} ions are the typical red source in upconversion, where Gd^{3+} is used as an intermediary bridge rather than Yb^{3+} because of the mismatch of energy levels between Yb^{3+} and Eu^{3+}. Upon co-doping Eu^{3+} into the core, however, the red emissions of Eu^{3+} are quenched by Tm^{3+} and Er^{3+} (Figure S7). The problem was solved by coating $NaGdF_4$:Eu onto the $NaGdF_4$:Yb/Er/Tm core to obtain the desired energy-migration pathway of red emissions: $Yb^{3+} \rightarrow Tm^{3+} \rightarrow Gd^{3+}$(core)$\rightarrow Gd^{3+} \rightarrow Eu^{3+}$(shell) (Figure 1 a). When the proportion of Eu^{3+} in the shell reached 10 mol%, pure white light was obtained by combining the Eu^{3+} emission with the blue and green emissions of core (Figure S8).

Interestingly, we observed that the emission colors can be dynamically tuned by changing the excitation power density of a 980 nm laser (Figure 2 a and Figure S9). The emission colors showed a continuous evolution from green to cyan to white and to red with power densities from 3 to 30 W cm^{-2}. When we loaded the nanocrystals into polystyrene microbeads, the beads similarly showed the four typical colors under the excitations of 3, 10, 15, and 30 W cm^{-2} (Figure 2 b). From the upconversion spectra at different excitation power densities, the calculated chromaticity coordinates shown by the sequence of color evolution are in agreement with our observations with the naked eye (Figure S10 and Table S1).

In order to obtain a better understanding of the color evolution, we deconvoluted the spectral bands into individual Gaussian peaks, and divided them into three groups: blue from 400 to 500 nm, green from 500 to 575 nm, and red from 575 to 750 nm (Figure 3 a and Table S2). A series of upconversion spectra at different excitation power densities were measured, and the integrated intensity of each peak was calculated. The three color intensities increased as the laser power density increased, but exhibited very different increase rates, namely red > blue > green (Figure 3 b), leading to a change of proportions of the three colors in the total emission intensity (Figure 3 c). The percentage of the red emission rapidly increased from 10 to 55%, and contrarily, that of the green emission rapidly decreased from 60 to 15%

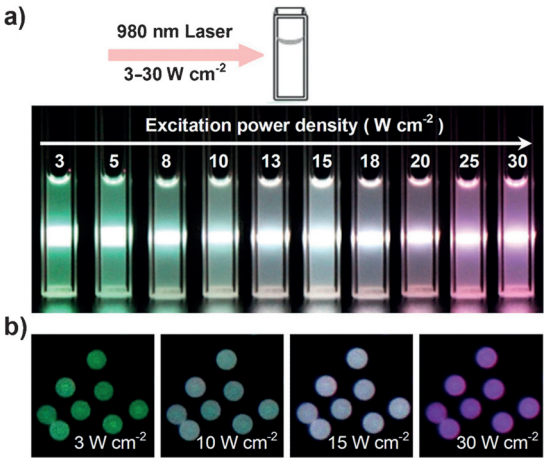

Figure 2. a) Luminescence of nanocrystals in cyclohexane (1 mg mL^{-1}). The photos were taken in the dark; a 980 nm laser with a power density of 3 to 30 W cm^{-2} was used to excite the same sample. b) The polystyrene microbeads (ca. 10 μm) loaded with the nanocrystals show four typical colors (from left to right: green, cyan, white, and red) under the indicated excitation power densities.

with the increase of power density from 3 to 30 W cm^{-2}. At the same time, the proportion of the blue emission remained almost constant at 30%. The proportion of the red emission clearly evolved from much lower to much higher relative to that of the green emission, and thus the change in the composition of the emitted light essentially caused the color evolution shown in Figure 2.

The photon-transfer pathways provide a mechanistic explanation for the formation of the emission colors (Figure 3d). Firstly, the $^4I_{11/2}$ level of the Er^{3+} ions best matches the $^2F_{5/2}$ level of Yb^{3+}, and the energy absorbed by Yb^{3+} transfers to Er^{3+} ions at a low excitation power density, leading to the predominantly green emission. Subsequently, the increase in power density results in the limited growth in the number of excited photons for Er^{3+} because of its very low doping concentration (0.05 mol%), and thus more energy is transferred to Tm^{3+} (0.5 mol%) to enhance the blue emission, which mixes with the green emission from the Er^{3+} ions to produce the cyan emission. Finally, a higher power density activates the higher energy levels of Tm^{3+} (from $^1G_4$ to $^1D_2$ to $^1I_6$), and transfers the energy through the Gd^{3+} $^6P_{7/2}$ level to the Eu^{3+} ^5D_j level (in the middle shell) to generate the red emission.[12,13] This is why the proportions of the RGB emissions clearly change with excitation power.

Moreover, the multiphoton processes were confirmed by linear fits of the logarithm of the integral intensity versus excitation power density, where the slope represents the number of excitation photons (Figure 3e). The slopes for green and blue emissions were 1.92 and 3.81 at power densities lower than 10 W cm^{-2}, thus showing the two-photon and four-photon processes, respectively. At higher excitation

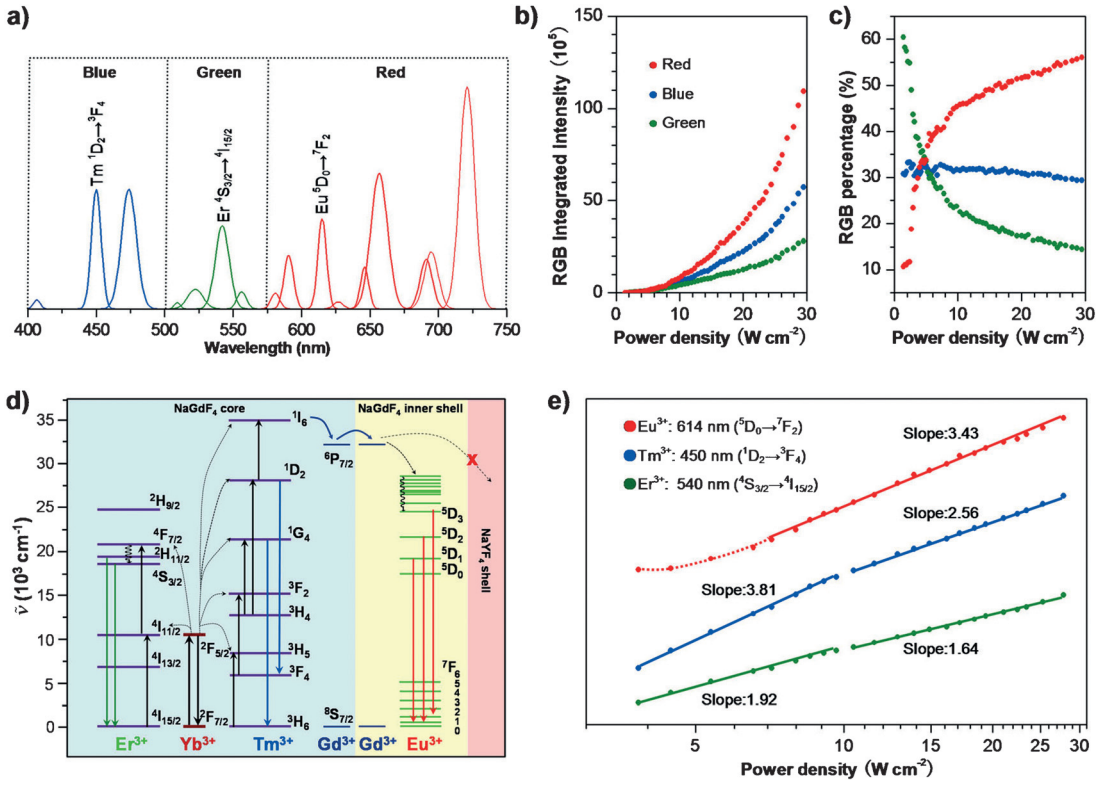

Figure 3. a) Deconvolution of a typical white-light spectrum into individual Gaussian peaks. b) RGB integrated intensities of red (575–750 nm), green (500–575 nm), and blue (400–500 nm) emissions as a function of excitation power density. c) Percentages of RGB intensity in the total spectral intensity as a function of excitation power density. d) Multiphoton transfer pathways and color origins in upconversion. e) Dependence of emission intensities on excitation power density for three typical color peaks at 614 nm (red: $^5D_0 \rightarrow {}^7F_2$ of Eu^{3+}), 450 nm (blue: $^1D_2 \rightarrow {}^3F_4$ of Tm^{3+}), and 540 nm (green: $^4S_{3/2} \rightarrow {}^4I_{15/2}$ of Er^{3+}).

powers, the slopes were reduced to 1.64 and 2.56, respectively, because of the restriction of accepting the excitation energy from the Yb^{3+} ions.[14] Meanwhile, the slope of the red emission at power densities higher than 8 $W cm^{-2}$ remained at 3.43. The excitation power density thus governs the photon-transfer pathways and changes the output of the emission colors.

Figure 4a shows a prototype concept of a flat-panel display on a nanocrystal-coated substrate. Pixels with different colors can be produced by fast scanning of a laser that is synchronously modulated by controlling the pump current. As a proof of concept, a display comprising an array of colored dots was successfully fabricated by loading the nanocrystals into etched microwells on a piece of silicon wafer and exciting every site with different laser power (Figure 4b), which was performed by using a customized system (Figure S11). We subsequently fabricated a prototype of a flat-panel display by using the color-tunable nanocrystals. Bamboo, panda, and rose motifs were printed onto standard A4 paper by an inkjet printer that used our colloidal nanostructure as colorless ink.[15] The green bamboo and white-black panda appeared on the paper when laser power densities of 3 and 15 $W cm^{-2}$ were used, respectively. Moreover, a rose with red petals and green stem and leaves was visible upon the synchronous use of two laser powers (Figure 4c).

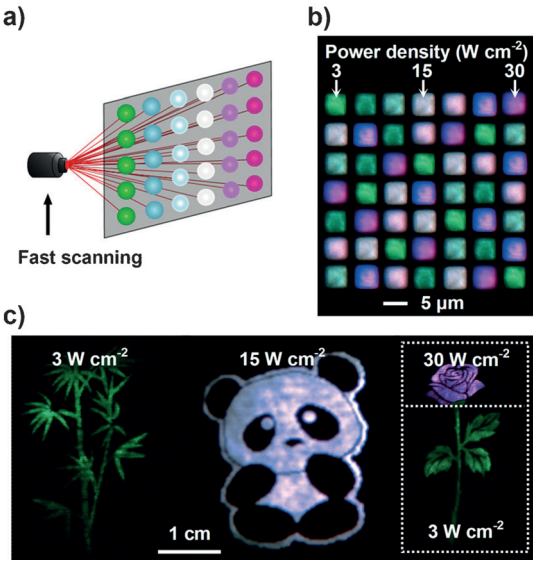

Figure 4. a) Concept for flat-panel display by the fast scanning of a laser with modulated power. b) Dot-array display on a piece of silicon wafer (the upconversion nanocrystals were loaded into 5×5 μm etched microwells on a silicon wafer). c) Pictures of bamboo, panda, and rose printed on a piece of A4 paper with an inkjet printer using the colloidal nanostructure as colorless ink.

We also showed another advantage of color-tunable nanocrystals in imaging by using *C. elegans* as an example.[16] The nanocrystals were modified with hydrophilic polymers (Figure S12) and then fed to WS4581 type *C. elegans*. The nanocrystals in the pharynxes and intestines of *C. elegans* can clearly be seen by their green, white, and red emissions at different excitation powers (Figure 5a). Meanwhile, the N2 and WS4581 types of *C. elegans* were fed with fixed-color green nanocrystals ($NaYF_4$:Yb/Er; Figure S13) and our color-tunable nanocrystals, respectively, and then they were mixed in the same medium. At a power density of 3 $W cm^{-2}$, both showed a green color in pharynxes and intestines. At 20 $W cm^{-2}$, however, they were clearly distinguishable in the same image: the N2 type remained green and the WS4581 type stayed red. In other imaging methods, the use of multiple fluorescence tags is required, which can lead to spectral interference. A further application of the nanostructures is shown in Figure S14.

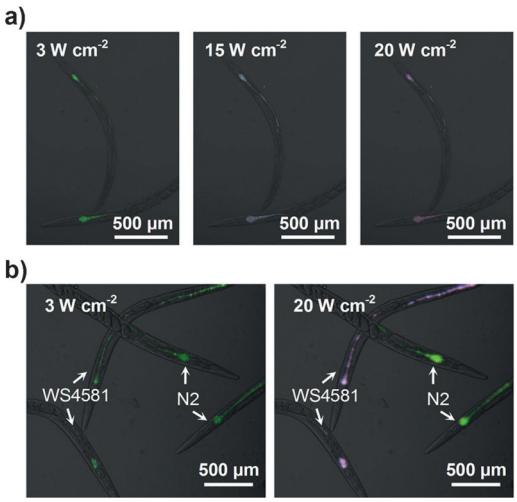

Figure 5. a) Imaging of *C. elegans* using three typical excitation power densities. b) Discrimination of two types *C. elegans* (N2 and WS4581) using different excitation power densities.

In summary, we have demonstrated that the incorporation of RGB-emitting lanthanide ions into a single nanostructure results in an emission across the whole of the visible spectrum, and the balanced intensities of the multiple upconversion emissions generates a bright white light. The regulated multiphoton pathways are governed by the excitation power density and allow each of the RGB chromophores to emit its characteristic wavelength independently. The response to excitation power density provides a very simple and convenient approach to tuning the emission colors. As evidenced by our results, the prototype color flat-panel display could be produced very simply by coating the nanocrystals onto a substrate and integrating a fine, power-tunable laser beam. In comparison with conventional fixed-color dyes or quantum dots, the use of color-tunable nanostructure as biological tags can also significantly improve the reliability and convenience of imaging. We believe that this new class of upconversion nanostructures will result in applications in displays, biological imaging, chemical sensing, and anticounterfeiting.

Acknowledgements

This work was supported by the National Basic Research Program of China (2015CB932002), National Key Technology R&D Program (2012BAJ24B02), National Natural Science Foundation of China (21335006, 21475135, 21375131) and Natural Science Foundation of Anhui Province (1408085MKL52).

Keywords: lanthanides · nanostructures · photochemistry · upconversion · white light

How to cite: *Angew. Chem. Int. Ed.* **2015**, *54*, 11531 – 11535
Angew. Chem. **2015**, *127*, 11693 – 11697

[1] R. W. Sabnis, *Displays* **1999**, *20*, 119 – 129.
[2] a) S. Mukherjee, P. Thilagar, *Dyes Pigm.* **2014**, *110*, 2 – 27; b) G. He, D. Guo, C. He, X. Zhang, X. Zhao, C. Duan, *Angew. Chem. Int. Ed.* **2009**, *48*, 6132 – 6135; *Angew. Chem.* **2009**, *121*, 6248 – 6251.
[3] a) E. Jang, S. Jun, H. Jang, J. Lim, B. Kim, Y. Kim, *Adv. Mater.* **2010**, *22*, 3076 – 3080; b) Y. Shirasaki, G. J. Supran, M. G. Bawendi, V. Bulović, *Nat. Photonics* **2012**, *7*, 13 – 23.
[4] S. Sivakumar, F. C. van Veggel, M. Raudsepp, *J. Am. Chem. Soc.* **2005**, *127*, 12464 – 12465.
[5] a) Y. J. Hong, C. H. Lee, A. Yoon, M. Kim, H. K. Seong, H. J. Chung, C. Sone, Y. J. Park, G. C. Yi, *Adv. Mater.* **2011**, *23*, 3284 – 3288; b) R. Deng, F. Qin, R. Chen, W. Huang, M. Hong, X. Liu, *Nat. Nanotechnol.* **2015**, *10*, 237 – 242.
[6] a) W. C. Chan, D. J. Maxwell, X. Gao, R. E. Bailey, M. Han, S. Nie, *Curr. Opin. Biotechnol.* **2002**, *13*, 40 – 46; b) P. Zrazhevskiy, X. Gao, *Nat. Commun.* **2013**, *4*, 1619.
[7] a) F. Wang, X. Liu, *Acc. Chem. Res.* **2014**, *47*, 1378 – 1385; b) J. Zhou, Q. Liu, W. Feng, Y. Sun, F. Li, *Chem. Rev.* **2015**, *115*, 395 – 465.
[8] a) F. Wang, Y. Han, C. S. Lim, Y. Lu, J. Wang, J. Xu, H. Chen, C. Zhang, M. Hong, X. Liu, *Nature* **2010**, *463*, 1061 – 1065; b) J. C. Boyer, F. Vetrone, L. A. Cuccia, J. A. Capobianco, *J. Am. Chem. Soc.* **2006**, *128*, 7444 – 7445; c) F. Wang, X. Liu, *J. Am. Chem. Soc.* **2008**, *130*, 5642 – 5643; d) H. X. Mai, Y. W. Zhang, L. D. Sun, C. H. Yan, *J. Phys. Chem. C* **2007**, *111*, 13721 – 13729; e) M. Haase, H. Schäfer, *Angew. Chem. Int. Ed.* **2011**, *50*, 5808 – 5829; *Angew. Chem.* **2011**, *123*, 5928 – 5950; f) F. Wang, X. Liu, *Chem. Soc. Rev.* **2009**, *38*, 976 – 989.
[9] a) Q. Su, S. Han, X. Xie, H. Zhu, H. Chen, C. K. Chen, R. S. Liu, X. Chen, F. Wang, X. Liu, *J. Am. Chem. Soc.* **2012**, *134*, 20849 – 20857; b) G.-S. Yi, G.-M. Chow, *Chem. Mater.* **2007**, *19*, 341 – 343; c) H. Schäfer, P. Ptacek, O. Zerzouf, M. Haase, *Adv. Funct. Mater.* **2008**, *18*, 2913 – 2918.
[10] H. S. Qian, Y. Zhang, *Langmuir* **2008**, *24*, 12123 – 12125.
[11] D. Chen, Y. Wang, K. Zheng, T. Guo, Y. Yu, P. Huang, *Appl. Phys. Lett.* **2007**, *91*, 251903.
[12] F. Wang, R. Deng, J. Wang, Q. Wang, Y. Han, H. Zhu, X. Chen, X. Liu, *Nat. Mater.* **2011**, *10*, 968 – 973.
[13] J. Zhao, D. Jin, E. P. Schartner, Y. Lu, Y. Liu, A. V. Zvyagin, L. Zhang, J. M. Dawes, P. Xi, J. A. Piper, E. M. Goldys, T. M. Monro, *Nat. Nanotechnol.* **2013**, *8*, 729 – 734.
[14] J. Suyver, A. Aebischer, S. García-Revilla, P. Gerner, H. Güdel, *Phys. Rev. B* **2005**, *71*, 125123.
[15] Q. Mei, Z. Zhang, *Angew. Chem. Int. Ed.* **2012**, *51*, 5602 – 5606; *Angew. Chem.* **2012**, *124*, 5700 – 5704.
[16] a) S. F. Lim, R. Riehn, W. S. Ryu, N. Khanarian, C. K. Tung, D. Tank, R. H. Austin, *Nano Lett.* **2006**, *6*, 169 – 174; b) N. Mohan, C. S. Chen, H. H. Hsieh, Y. C. Wu, H. C. Chang, *Nano Lett.* **2010**, *10*, 3692 – 3699.

Received: May 19, 2015
Revised: June 29, 2015
Published online: July 23, 2015

